Needle Localization and Segmentation for Radiofrequency Ablation of Liver Tumors under CT Image Guidance

Le Quoc Anh[1], Luu Manh Ha[1,2,3,*], Theo van Walsum[3], Adriaan Moelker[3], Dao Viet Hang[4,5], Pham Cam Phuong[6], and Vu Duy Thanh[1]

[1]*AVITECH, VNU University of Engineering and Technology, Hanoi, Vietnam*
[2]*FET, VNU University of Engineering and Technology, Hanoi, Vietnam*
[3]*Department of Radiology and Nuclear Medicine, Erasmus MC, Rotterdam, the Netherlands*
[4]*Internal Medicine Faculty, Hanoi Medical University, Hanoi, Vietnam*
[5]*The Institute of Gastroenterology and Hepatology, Vietnam*
[6]*The Nuclear Medicine and Oncology center, Bach Mai hospital, Hanoi, Vietnam*
[*]*Corresponding author email: halm@vnu.edu.vn*

***Abstract*—Radiofrequency ablation (RFA) of liver cancer under computer tomography (CT) guidance is a minimally invasive procedure in which CT images are utilized to guide the physician in introducing the needle into the target lesion. However, the adequate visualization of the needle and anatomy is hampered by the 2D slide based-view used in the current clinical practice. Thus, due to the lack of 3D information, the physician requires high experience and more interaction with the guidance systems to envision the needle's position in the liver, which is inconvenient in clinical practice. In this study, we propose a method for robust needle segmentation using CT images to improve the visualization of the needle during the intervention. The method utilizes a convolutional neural network (CNN) to detect the needle in orthogonal 2D projections of the CT image to construct the needle volume of interest (VOI). Subsequently, a patch-based 3D CNN is applied to segment the needle. We evaluate the method's accuracy using Dice score (DSC), Hausdorff distance (HD), the needle shaft error E_{shaft}, and needle tip error E_{tip}. The results show that the proposed method achieves the means of DSC, HD, E_{tip}, E_{shaft} and processing time of 0.89, 3.3 mm, 0.9 mm, 0.43 mm, and 2.6 seconds, respectively. We conclude that the proposed method is feasible for improving needle visualization in the interventional room.**

***Index Terms*—Liver tumors, RFA, needle segmentation, CT guidance, projections, CNN**

I. Introduction

Radiofrequency ablation (RFA) for liver cancer treatment is an effective curative therapy at an early stage, especially for patients unsuitable for operation indications [1]. In the RFA procedure, an interventional physician inserts a needle into the patient with the tip at the tumor to destroy the malignant tissue. The needle delivers the radiofrequency waves (350–500 kHz) directly to the surrounding tissue, leading to tissue necrosis [2]. RFA is a minimally invasive procedure with a low risk of death and low-risk complications during the treatment. Moreover, RFA is a relatively quick, repeatable, and low-cost procedure, and patients can be discharged in a few days after the intervention [3].

Local tumor progression is a major factor limiting the effectiveness of RFA for liver cancer treatment, with a reported local recurrence rate ranging from 15 to 40% [4]. The success of the technique decreases when treating the tumors of larger than 3 cm since the tumors may be not covered within the thermal ablation [2]. The local recurrence rate also increases when performing RFA with the tumor abutting large vessels (larger than 3 mm in diameter). These vessels may lead to insufficient ablation, caused by the heat-sink effect of the vessels [1], [4]. Thus, accurate needle placement is needed to improve treatment efficiency, minimizing the limitation of RFA.

RFA under CT guidance is frequently used for liver cancer treatment since CT images provide adequate information on the needle position [5]. Currently, with details from CT images, the physician manually determines the angle and direction to insert the tip of the needle toward the target position. However, to guarantee the adequacy of the needle placement, the physician often repositions the needle multiple times, increasing the chance of complications (e.g., bleeding, tract seeding) [6]. Moreover, in the current clinical practice, the 2D slide based-view of CT image is often used to adjust the needle placement, which requires high operator experience and might be time-consuming. In addition, the intra-interventional CT images are usually non-contrast enhanced and with fewer slices to reduce the patient's risk of renal impairment and radiation exposure during the procedure, leading to low image quality. Therefore, the physician needs numerous interactions with the system to ensure an adequate position [6]. Additionally, several studies have proposed robotics for guiding treatment in the intervention room, showing the potential of needle segmentation in clinical practice [1], [7]. Thus, a 3D

978-616-590-477-3 ©2022 APSIPA APSIPA ASC 2022

modeling of the needle could benefit both the physician and a robotic approach during the puncture procedure, which may improve procedural convenience and treatment accuracy by providing the 3D information to visualize the position of the needle.

The needle segmentation in the CT image during the RFA procedure is the main challenge to perform the 3D needle modeling. However, there are several challenges for computers to segment the needle in CT images accurately (see Fig. 1): (1) The needle in the CT image is usually displayed in a few slices only with low resolution and low image quality due to the purpose of reducing the radiation exposure to the patients; (2) Metal artifacts caused by the needle potentially add noise to the needle boundary, thus it is difficult to separate the needle from the liver parenchyma; (3) The needle in CT images has the same range of intensity values as other structures such as bone or other metal equipment attached to the patient; (4) The size and direction of the needle are different for each patient, resulting in the various size of needle-VOI; (5) The processing time is also an essential factor that helps minimize the duration of treatment.

In this paper, we propose and assess a method for needle segmentation in the CT image. Our approach is to utilize two CNNs for localization and segmentation of the needle, aiming for speed and accuracy. The 3D needle localization problem can be solved by using 2D needle detection in three orthogonal maximum intensity projections (MIPs) utilizing a one-stage detector-YOLOv4 [8] to construct the needle-VOI. A transfer learning-based CNN approach is applied to segment the needle in the needle-VOI, in which the weight of the segmentation network is transferred from the CNN introduced by Mehrtash *et al.* (MehrtashNet) [7]. We also investigate the optimal parameters for the proposed method to take advantage of the localization and segmentation networks. The results show that the proposed method achieved compatible accuracy and significantly less processing time than other state-of-the-art methods.

The remainder of this paper is organized as follows: We review several related studies to our work in section III. The details of the proposed method are described in section III. Section IV covers the experiment and results of the study. Finally, we discuss and conclude the findings of this study in section V.

II. Related Work

Many studies for needle segmentation and localization have been published. Based on clinical application, the methods are proposed for solving problems related to puncture, ablation, biopsy, and brachytherapy and are also applied in different image modalities, including ultrasound (US), magnetic resonance imaging (MRI), and CT. These methods can be catagorized into two groups: traditional image processing methods and deep learning approaches.

A. Traditional image processing methods for needle segmentation and detection

Hough transform and Radon transform are often applied to detect linear objects, which are utilized in various needle tracking studies. Qui *et al.* developed a method of needle segmentation in 3D transrectal US, and this method improves the implementation of the Hough transform to reduce needle detection time [9]. Zheng *et al.* introduced a technique based on an improved Hough transform to detect the ablation needle and its tip in CT images [10]. Hatt *et al.* utilized the Radon transform to extract the position and orientation of the needle in the 2D beam-steered US [11]. Studies mentioned above deal with straight needles. Meanwhile, the needle can be curved when performing the RFA procedure due to the flexible needles and movement of the patient's organ [12].

The projection-based approach is often chosen for estimating the needle position and orientation. Alpers *et al.* introduced an image processing pipeline for needle position and orientation reconstruction in the CT image during the RFA procedure [6]. Their method is a combination of projection-based and morphological approaches to reduce the computational time. However, this method uses the projection-based approach to provide 2D information for the physician so that it can be error-prone due to the lack of 3D information. Aboofazeli *et al.* presented a method based on the projection and Hough transform to address curved needle detection in 3D US images [12]. This method applied Hough transform to detect the needle, which is unsuitable when other structures have a shape that looks like needle the in the image [6].

B. Deep learning approach for needle segmentation and detection

In recent years, deep neural networks have been applied to solve many tasks in medical image analysis and yielded much more competitive results than traditional methods [7]. Deep learning techniques also have been investigated to support the physician in the interventional room, showing potential to apply in clinical practice. Arif *et al.* (2019) utilized a CNN based on V-net to segment the needle in 3D US images [13]. Zhang *et al.* (2020) presented a deep learning model, a variant of the U-Net architecture, to segment the needle in 3D transrectal US images [14].

Although the mentioned deep learning-based methods have shown their efficiency in needle segmentation, these methods fed all image information into a CNN model, which might result in segment needle-like structure (e.g., radiopaque grid, metal wire...) and lead to increase computational cost. Mehrtash *et al.* (2018) introduced an automatic method for segmenting the needle in MRI images, supporting guidance prostate biopsy [7]. This method segments the prostate in MRI images by a 2D CNN to construct the VOI. Subsequently, the VOI of the prostate is fed into a 3D CNN to segment the needle. However, adding an additional segmentation framework to construct the VOI may increase the processing time. It was reported by Tian *et al.* that the segmentation of the prostate in 3D MRI requires about 4 seconds [15].

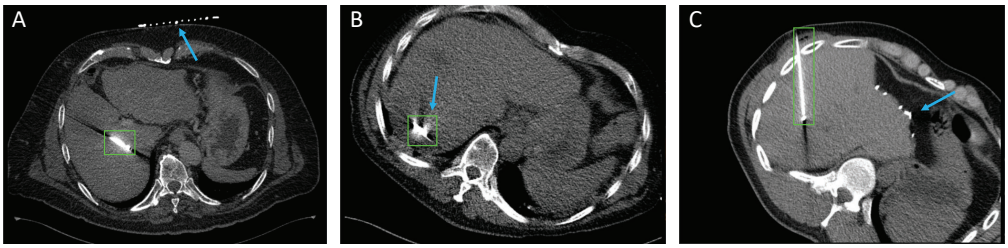

Fig. 1. Examples of intra-interventional CT images that contain the needle (in the green rectangles). Some challenges for needle segmentation (blue arrow) include A-radiopaque grid, B-needle artifact, and C-surgical clips.

III. Method

In this section, we will describe our proposed method that combines two CNNs for localization and segmentation tasks. Fig. 2 illustrates the proposed method's pipeline, which contains four steps. *Step 1*: Generate three orthogonal MIPs and detect the needle in these MIPs. *Step 2*: Generate the 3D bounding box by adding an expanded border to guarantee to cover all the needle area. *Step 3*: Generate the needle-VOI and separate it into multiple patches without overlapping. *Step 4*: Feed the patches into the segmentation network and perform world coordinate mapping of the prediction to get the final needle segmentation.

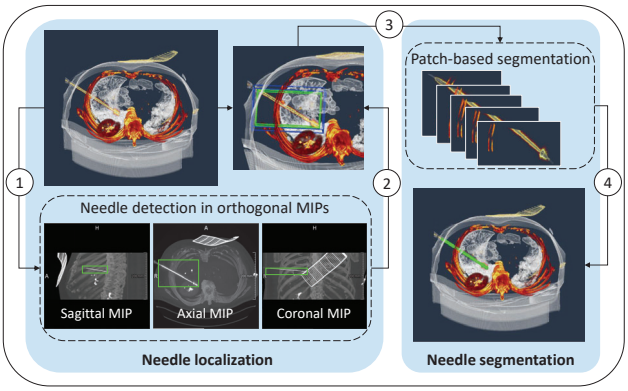

Fig. 2. The diagram of the proposed method for localizing and segmenting the needle in the CT image.

A. Needle localization

Performing the needle segmentation inside the needle-VOI may eliminate the irrelevant structures and objects in the CT image. The needle-VOI extraction is a 3D localization task. We transfer the 3D localization problem to 2D needle detection to reduce computational complexity. When performing CT imaging during the intervention, the needle strongly attenuates the photon beam and causes beam hardening, resulting in an area around the needle in the CT images with often streaks of high and low intensity values. [16]. MIP, a rendering technique that is widely used in medical image analysis, selects the highest intensity along the direction of the projection to create a 2D image. Therefore, MIP is suitable for highlighting the needle in contrast to soft tissue, helping to detect the needle accurately. The MIP of a CT image (ΔV) along the z-axis direction is obtained as follows:

$$\mathrm{MIP}\left(\Delta V^t(x,y)\right) = \max_z \Delta V^t(x,y,z). \tag{1}$$

We use YOLOv4 to detect the needle in the orthogonal MIPs since the YOLO-based approach is often applied in studies for object detection in medical image analysis, which requires a tight processing time [17]. A YOLO-based detector is a one-stage detector introduced for real-time object detection [8]. YOLOv4 has an optimized data processing and network architecture, balancing accuracy and processing time.

The CT image is projected along three directions (z-axis (axial), y-axis (sagittal), and x-axis (coronal)) to create three 2D orthogonal MIPs. The approximate needle tip position could be extracted from these orthogonal MIPs. Similar to the needle tip, we can determine the approximate starting position of the needle. From two approximated positions, we can generate the needle-VOI. Because the needle localization tasks may have some errors in extracting the volume covering the needle area, we will add an expanded border to the needle volume to obtain the final needle-VOI. The expanded border value is determined in Section IV.

B. Needle segmentation

Transfer learning is sometimes applied in medical image analysis fields due to the lack of clinical data [18]. The main idea of transfer learning is its ability to use previously trained knowledge (features, weights) for a new model for solving a similar problem. This approach may shorten the training process and improve the model's performance for the new task. Besides, transfer learning requires less training data, thus addressing the lack of data problem. In this study, we reuse the model for needle segmentation provided by Mehrtash *et al.* (MehrtashNet). MehrtashNet is inspired by the U-Net model, which consists of 14 convolution layers and three skip-connections. Because this architecture is designed with the input size of (188x188x46) and the prediction output size of (100x100x18), we use a patch-based strategy to segment the needle to overcome the various needle shapes while still taking advantage of the MehrtashNet architecture and transfer learning process by retraining the trained model from needle segmentation model for MRI image [19]. After

appyling MehrtashNet to determine the needle segmentation, we keep the largest connected component to get the final needle segmentation.

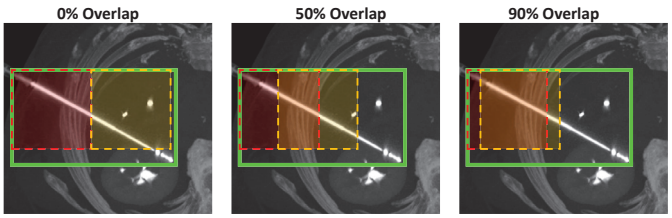

Fig. 3. Example of patch separation with null, medium, and high extent of overlap. The green rectangle represents the needle-VOI, the red and orange areas corresponding to the first and the following patches.

One issue that needs to be mentioned in the patch-based segmentation strategy is the extent of overlap [19]. Fig. 3 shows the patch separation with three extents of overlap, indicating that with the large extent value, there is more sample provided for the model to segment, resulting in more information and increasing the processing time. The optimal extent of overlap will be determined via the experiment in Section IV.

IV. Experiment and Evaluation

A. Data and annotations

The data used in this study was reused from our previous work [20], consisting of 111 intra-interventional CT images obtained from 24 patients that underwent RFA with CT image guidance. The images were anonymized before being used in this study. The CT images were obtained from Siemens CT scanners with a low-dose protocol, the in-plane resolution ranges from 0.51 to 0.92 mm, and the slice thickness ranges from 0.4 mm to 5 mm, with the number of slices from 14 to 501. The CT images were acquired at 80-120 kVP, with CTDIvol 2-10 mGy. The needle annotation is labeled by a technician using the region growing algorithm and manually edited the mislabeled, which is referred as the ground truth. The needle segmentation ground truth is then verified by an expert.

TABLE I
Number of CT image data for training/validation and testing

set	Training/validation		Testing	
	#Images	#Slices	#Images	#Slices
size	88	5606	23	1272

The dataset was randomly splitted by 80% for training/validation of the proposed framework and by 20% for testing the performance of the proposed method. The characteristics of the splitted datasets are summarized in Table I.

B. Implementation Detail

This study was conducted on a workstation with Ubuntu 20.04 operating system with an Intel i9 10900K processor, 10 cores, and 20 threads with a clock rate of 3.7 – 5.3 GHz, 64GB RAM, and an RTX 3090 24GB VRAM GPU. Deep learning models are run with the CUDA 11.2 library. The object detector, YOLOv4, was implemented in the Darknet framework [8], based on the open-source code of the author's Github repository. MehrtashNet is implemented in the Keras (version 2.8.0) with Tensorflow (version 2.8.0) backend. The proposed method is written in Python version 3.8.

We trained YOLOv4 using the fine-tuning technique, and the pre-trained model was trained on the MS COCO dataset. The training data consists of 264 orthogonal MIPs. In the preprocessing step, the orthogonal MIPs intensity is clipped to the range 400 to 3072, then scaled to the range of 0 to 255. Data augmentation techniques include random rotation (0, 90, 180 and 270 degree), changing the contrast (in a range of 1.0 to 1.5), and adding Gaussian noise (with sigma value of 0.1). We trained the YOLOv4 model with 100 epochs, using an image size of 512x512, and batch size of 8 images, with a learning rate, momentum, and decay set of 1×10^{-3}, 0.9, and 5×10^{-5}, respectively. The training loss function consists of three parts: Class loss, Box loss, and Object loss. To evaluate the performance of the localization task, we used two metrics, $3D\ IoU$ and wall distance (WD) [17].

To train MehrtashNet, we used the trained model for the needle segmentation task in MRI images [7]. Since the input size is 188x188x46 and the output is 100x100x18, we split patches in size of 100x100x18 in the needle-VOI area. To match MehrtashNet input size, we used zero padding to convert the input to 188x188x46 in size. In addition, we used Dice loss with SGD algorithm and Adam optimization as suggested in the original paper. The training parameters are reused from the original paper.

For performance comparison with the proposed method, we implemented the nn-Unet framework based on the open-source code from the author's Github repository [21]. The advantage of nn-Unet is that it can automatically self-configure based on the input dataset, which enables nn-Unet to achieve high rankings in various medical imaging competitions. We trained nn-Unet with the same training/validation set as the proposed method.

C. Evaluation metrics

Two standard metrics used to evaluate the accuracy of the segmentation task, the Dice score (DSC) and the Hausdorff distance (HD), are used in this study. The DSC is calculated as follows:

$$DSC = \frac{2|X \cap Y|}{|X| + |Y|}, \tag{2}$$

where X and Y is the predicted segmentation and ground truth segmentation. The HD can be defined as follows:

$$HD(X,Y) = \max\left\{\max_{\mathbf{x}\in X}\min_{\mathbf{y}\in Y} d(\mathbf{x},\mathbf{y}), \max_{\mathbf{y}\in Y}\min_{\mathbf{x}\in X} d(\mathbf{x},\mathbf{y})\right\}, \tag{3}$$

where $d(\mathbf{x},\mathbf{y})$ is Euclidean distance between two points $\mathbf{x}$ and $\mathbf{y}$.

In clinical practice, the needle shaft and tip positions are two major factors in measuring the method's performance. Based on the study of Zhang *et al.* [14], the needle shaft error (E_{shaft}) and needle tip error (E_{tip}) are used. We calculate the E_{shaft} as follows:

$$E_{shaft} = \frac{1}{N}\sum_{i=1}^{N} d\left(\boldsymbol{CX}_i, \boldsymbol{CY}_i\right), \tag{4}$$

where N is the number slice that contains the needle in an image, $\boldsymbol{CX}_i$ and $\boldsymbol{CY}_i$ are the predicted and ground truth position of the center of mass of the needle for the ith slice. The E_{tip} is defined as:

$$E_{tip} = \frac{1}{M}\sum_{i=1}^{M} d\left(\boldsymbol{TX}_i, \boldsymbol{TY}_i\right), \tag{5}$$

where M is the number of needles in an image, $\boldsymbol{TX}_i$ and $\boldsymbol{TY}_i$ are the tip position of predicted and ground truth in the ith needle.

D. Evaluation of needle localization accuracy and determine expanded border value

We evaluated the accuracy of localizing the needle in the CT image. The YOLOv4 successfully detected the needle on orthogonal MIPs in 22 out of 23 CT images of the test set. The localization algorithm achieved a mean $3D\ IoU$ score of 77% and the WD of 3.6 mm. Moreover, the algorithm estimated the 3D bounding box in 0.04 seconds on average. The algorithm defines the 3D bounding box with the largest missing range of needle area as 8.2 mm, and the largest excess range of needle area as 31.2 mm. Therefore, we chose the expanded border value of 10 mm to guarantee the needle inside the needle-VOI.

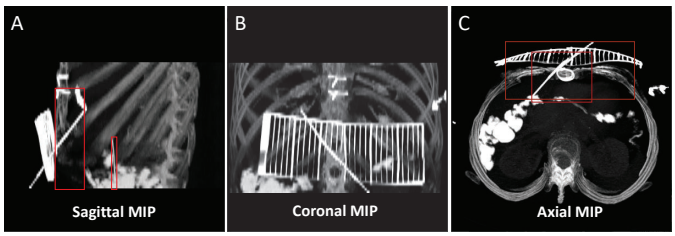

Fig. 4. A failure localization case in which the object detector results in the prediction with a lower confidence score where the radiopaque grid projection is overlapped the needle projection. The red bounding box represents a confidence score lower than 10%.

Fig. 4 shows the results of a case when the YOLOv4 detects the needle with low confidence, resulting in a failure in needle-VOI estimation. In this case, a technician manually draws the bounding box in the orthogonal MIPs to create the needle-VOI for further evaluation.

E. Needle segmentation

1) Define the optimal extent of overlap value: To determine the optimal extent of overlap value, we use the needle 3D bounding box of ground truth to create the needle-VOI. As suggested by the study by Bernal *et al.* [19], we separate the patches in the needle-VOI area with null, medium, and high extent of overlap (see Fig. 3). Then, we fed the patches into the proposed needle segmentation flow to obtain the needle segmentation.

TABLE II
COMPARISONS OF THE AVERAGES OF THE ACCURACY AND PROCESSING TIME (PT) WHEN VARYING THE EXTENT OF OVERLAP VALUE WITH NULL, MEDIUM, AND HIGH VALUES.

Metrics	DSC	HD	E_{shaft}(mm)	E_{tip}(mm)	PT (s)
null	0.89	2.8	0.39	0.78	1.8
medium	0.89	2.8	0.39	0.8	3.2
high	0.88	3.7	0.4	0.75	83

Table II displays accuracy and processing time when varying the extent of overlap value. Using Student's t-Test, we found no significant difference between the accuracies of the extent of overlap values (p-value>0.1). Meanwhile, the lowest average processing time reached 1.8 seconds at the null extent of overlap value. Therefore, we chose the null extent of overlap value for the following evaluation step.

2) Evaluation of needle segmentation accuracy: We compare the accuracy and processing time of the proposed method with state-of-the-art methods. The proposed method used the expanded border value of 10 mm and the null extent of overlap value to segment the needle in the CT images. MehrtashNet uses all image information and performs patch-based segmentation with the null extent value. Fig. 5 shows that using all image information leads to unwanted segment regions. We manually select the connected component of the nn-UNet and MehrtashNet needle regions to compare with the proposed method. Table III indicated that the proposed method achieved comparable accuracy, while the processing time is significantly lower than state-of-the-art methods.

TABLE III
COMPARISONS OF THE MEDIANS OF ACCURACY AND PROCESSING TIME (PT) OF THE STATE-OF-THE-ART NEEDLE SEGMENTATION METHODS ON CT IMAGES.

Metrics	DSC	HD	E_{shaft} (mm)	E_{tip} (mm)	PT (s)
Proposed method	0.89	3.3	0.43	0.9	2.6
MehrtashNet + CC*	0.87	5.5	0.61	3.1	33
nn-Unet + CC*	0.89	1.9	0.56	0.5	28

* *manually select the connected component (CC) to get final needle segmentation.*

V. DISCUSSIONS AND CONCLUSIONS

The performance of the needle localization task is presented in sections IV-D. The proposed method achieved 77% of $3D\ IoU$ and 3.6 mm of WD. YOLOv4 is a convolutional neural network that is data-driven; thus, performance could be improved when there is a larger amount of data in the training process. However, collecting large amounts of data is a challenge. Therefore, how to improve the performance of the localization task with limiting data will be a topic of future research.

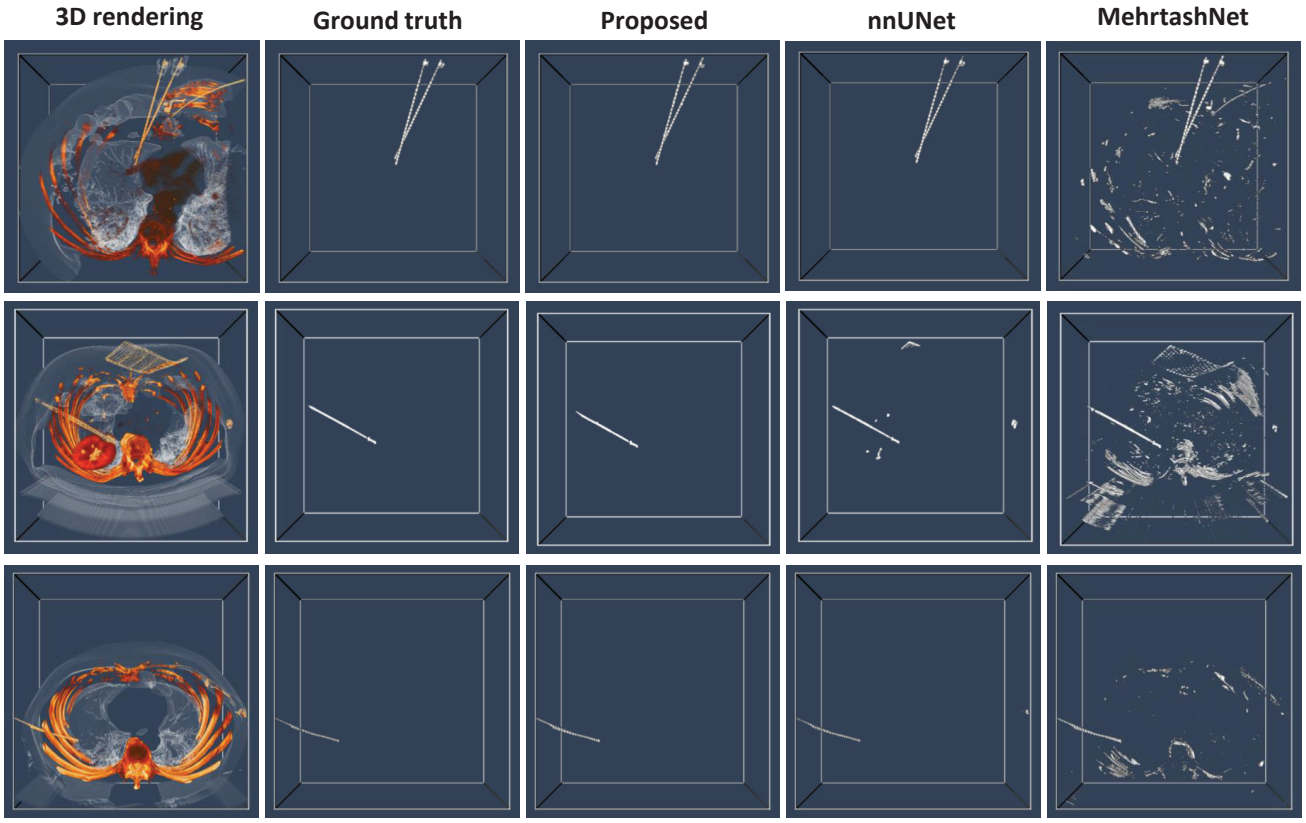

Fig. 5. Examples of needle segmentation in the testing set (first row: two-needle; middle row: needle and radiopaque grid; last row: curved needle). The first column is the 3D rendering of the CT image, and the following column is the ground truth of needle segmentation and predicted segmentation from the methods in this study.

Table II shows that when performing the needle segmentation in an accurate needle-ROI (i.e., ground truth), the performance of the proposed method is improved. First, the smaller needle-VOI reduces the processing time (1.8 seconds). Compared to the results from Table III, the proposed method with adding the expanded border value and the error of localization task, leading to larger needle-VOI, has increased processing time (2.6 seconds). It can be seen that the patched-based segmentation strategy is affected by the needle-VOI. The accuracy is decreased when a larger needle-VOI is performed.

Table III shows that the proposed method requires significantly less processing time than the state-of-the-art methods. These results indicate that performing segmentation in the needle-VOI reduces the processing time compared to using the whole image. In addition, Fig. 5 shows that irrelevant structures are eliminated using the proposed method.

In clinical practice, if the needle tip position and the target position is larger than 5 mm apart, the physician or robot needs to reposition the needle to get an adequate position [1]. The needle tip error of the proposed method archived a mean accuracy of 0.9 mm, and thus it is acceptable in term of accuracy.

This study still has some limitations. First, we did not improve needle detection in orthogonal projections and used an expanded border value to guarantee the needle into needle-VOI. The expanded border value may depend on the detector's performance and the dataset's quality. Secondly, if the needle is placed in-plane when generating the projections, the needle information is small, and it lacks of information to determine the needle-VOI area accurately. In a further study, this problem should be investigated more thoroughly.

In conclusion, this study has proposed a method for needle localization and segmentation in CT images to improve needle visualization in the RFA intervention procedure. We evaluated the performance of the needle localization task, which is the main contribution to the proposed method's advantages in reducing the processing time and eliminating unwanted regions segmentation. The results showed that the proposed method achieved comparable accuracy while having a significantly less processing time than the state-of-the-art methods. The results of this study show the potential to apply in clinical practice.

VI. Acknowledgments

This work has been supported by VNU University of Engineering and Technology under project number CN22.04. Le Quoc Anh was funded by Vingroup JSC and supported

by the Master, PhD Scholarship Programme of Vingroup Innovation Foundation (VINIF), Institute of Big Data, code VINIF.2021.ThS.95.

REFERENCES

[1] W. J. Heerink, S. J. Ruiter, J. P. Pennings, B. Lansdorp, R. Vliegenthart, M. Oudkerk, and K. P. de Jong, "Robotic versus freehand needle positioning in ct-guided ablation of liver tumors: a randomized controlled trial," *Radiology*, vol. 290, no. 3, pp. 826–832, 2019.

[2] P. Liu, J. Qin, B. Duan, Q. Wang, X. Tan, B. Zhao, P. L. Jonnathan, C.-K. Chui, and P.-A. Heng, "Overlapping radiofrequency ablation planning and robot-assisted needle insertion for large liver tumors," *The International Journal of Medical Robotics and Computer Assisted Surgery*, vol. 15, no. 1, p. e1952, 2019.

[3] I. Gory, M. Fink, S. Bell, P. Gow, A. Nicoll, V. Knight, A. Dev, A. Rode, M. Bailey, W. Cheung *et al.*, "Radiofrequency ablation versus resection for the treatment of early stage hepatocellular carcinoma: a multicenter australian study," *Scandinavian journal of gastroenterology*, vol. 50, no. 5, pp. 567–576, 2015.

[4] H. Takahashi, B. Kahramangil, and E. Berber, "Local recurrence after microwave thermosphere ablation of malignant liver tumors: results of a surgical series," *Surgery*, vol. 163, no. 4, pp. 709–713, 2018.

[5] R. Li, S. Xu, W. F. Pritchard, J. W. Karanian, V. P. Krishnasamy, B. J. Wood, and Z. T. H. Tse, "Anglenav: Mems tracker to facilitate ct-guided puncture," *Annals of biomedical engineering*, vol. 46, no. 3, pp. 452–463, 2018.

[6] J. Alpers, C. Hansen, K. I. Ringe, and C. Rieder, "Ct-based navigation guidance for liver tumor ablation." in *VCBM*, 2017, pp. 83–92.

[7] A. Mehrtash, M. Ghafoorian, G. Pernelle, A. Ziaei, F. G. Heslinga, K. Tuncali, A. Fedorov, R. Kikinis, C. M. Tempany, W. M. Wells *et al.*, "Automatic needle segmentation and localization in mri with 3-d convolutional neural networks: application to mri-targeted prostate biopsy," *IEEE transactions on medical imaging*, vol. 38, no. 4, pp. 1026–1036, 2018.

[8] A. Bochkovskiy, C.-Y. Wang, and H.-Y. M. Liao, "Yolov4: Optimal speed and accuracy of object detection," *arXiv preprint arXiv:2004.10934*, 2020.

[9] W. Qiu, M. Yuchi, M. Ding, D. Tessier, and A. Fenster, "Needle segmentation using 3d hough transform in 3d trus guided prostate transperineal therapy," *Medical physics*, vol. 40, no. 4, p. 042902, 2013.

[10] Y. Zheng, K. Liu, M. Chen, J. Li, and G. Zha, "A method on detection and location of the ablation needle in ct images," in *Proceedings of the Third International Symposium on Image Computing and Digital Medicine*, 2019, pp. 175–181.

[11] C. R. Hatt, G. Ng, and V. Parthasarathy, "Enhanced needle localization in ultrasound using beam steering and learning-based segmentation," *Computerized Medical Imaging and Graphics*, vol. 41, pp. 46–54, 2015.

[12] M. Aboofazeli, P. Abolmaesumi, P. Mousavi, and G. Fichtinger, "A new scheme for curved needle segmentation in three-dimensional ultrasound images," in *2009 IEEE International Symposium on Biomedical Imaging: From Nano to Macro*. IEEE, 2009, pp. 1067–1070.

[13] M. Arif, A. Moelker, and T. van Walsum, "Automatic needle detection and real-time bi-planar needle visualization during 3d ultrasound scanning of the liver," *Medical image analysis*, vol. 53, pp. 104–110, 2019.

[14] Y. Zhang, Y. Lei, R. L. Qiu, T. Wang, H. Wang, A. B. Jani, W. J. Curran, P. Patel, T. Liu, and X. Yang, "Multi-needle localization with attention u-net in us-guided hdr prostate brachytherapy," *Medical physics*, vol. 47, no. 7, pp. 2735–2745, 2020.

[15] Z. Tian, L. Liu, and B. Fei, "Deep convolutional neural network for prostate mr segmentation," in *Medical Imaging 2017: Image-Guided Procedures, Robotic Interventions, and Modeling*, vol. 10135. SPIE, 2017, pp. 417–422.

[16] O. k. Song, Y. E. Chung, N. Seo, S.-E. Baek, J.-Y. Choi, M.-S. Park, and M.-J. Kim, "Metal implants influence ct scan parameters leading to increased local radiation exposure: A proposal for correction techniques," *Plos one*, vol. 14, no. 8, p. e0221692, 2019.

[17] M. H. Luu, T. van Walsum, H. S. Mai, D. Franklin, T. T. T. Nguyen, T. M. Le, A. Moelker, D. L. Vu, N. H. Le, Q. L. Tran *et al.*, "Automatic scan range for dose-reduced multiphase ct imaging of the liver utilizing cnns and gaussian models," *Medical Image Analysis*, vol. 78, p. 102422, 2022.

[18] P. Coupeau, J.-B. Fasquel, E. Mazerand, P. Menei, C. Montero-Menei, and M. Dinomais, "Patch-based 3d u-net and transfer learning for longitudinal piglet brain segmentation on mri," *Computer Methods and Programs in Biomedicine*, vol. 214, p. 106563, 2022.

[19] J. Bernal, K. Kushibar, M. Cabezas, S. Valverde, A. Oliver, and X. Lladó, "Quantitative analysis of patch-based fully convolutional neural networks for tissue segmentation on brain magnetic resonance imaging," *IEEE Access*, vol. 7, pp. 89 986–90 002, 2019.

[20] H. M. Luu, C. Klink, W. Niessen, A. Moelker, and T. v. Walsum, "Non-rigid registration of liver ct images for ct-guided ablation of liver tumors," *PloS one*, vol. 11, no. 9, p. e0161600, 2016.

[21] F. Isensee, P. F. Jaeger, S. A. Kohl, J. Petersen, and K. H. Maier-Hein, "nnu-net: a self-configuring method for deep learning-based biomedical image segmentation," *Nature methods*, vol. 18, no. 2, pp. 203–211, 2021.